Microscale Generation of Entangled Photons without Momentum Conservation

C. Okoth[1,2,*], A. Cavanna,[1,2] T. Santiago-Cruz,[1,2] and M. V. Chekhova[1,2,3]

[1]*Max Planck Institute for the Science of Light, Staudtstraße 2, 91058 Erlangen, Germany*
[2]*University of Erlangen-Nürnberg, Staudtstraße 7/B2, 91058 Erlangen, Germany*
[3]*Department of Physics, M. V. Lomonosov Moscow State University, Leninskie Gory, 119991 Moscow, Russia*

We report, for the first time, the observation of spontaneous parametric down-conversion (SPDC) free of phase matching (momentum conservation). We alleviate the need to conserve momentum by exploiting the position-momentum uncertainty relation and using a planar geometry source, a 6 μm thick layer of lithium niobate. Nonphase-matched SPDC opens up a new platform on which to investigate fundamental quantum effects but it also has practical applications. The ultrasmall thickness leads to a frequency spectrum an order of magnitude broader than that of phase-matched SPDC. The strong two-photon correlations are still preserved due to energy conservation. This results in ultrashort temporal correlation widths and huge frequency entanglement. The studies we make here can be considered as the initial steps into the emerging field of nonlinear quantum optics on the microscale and nanoscale.

Spontaneous parametric down-conversion (SPDC) is a well-developed tool to produce entangled photons for practical applications, such as quantum imaging [1–3], quantum key distribution [4,5], and quantum metrology [6,7], as well as for tests of quantum mechanics [8]. So far, SPDC has exclusively been used in the phase-matched regime: when the emitted daughter photons conserve the momentum of the pump photon. Fulfilling the phase-matching condition restricts both the choice of nonlinear materials and the available states the daughter photons can occupy. This has prompted the search for SPDC with phase matching absent, in particular, in the emerging field of nanoscale generation of entangled photons [9–12]. In this Letter, we make the first steps in this direction: we generate entangled photons on a microscale and solve the problems caused by the small size of the source.

For SPDC, the probability of a pump photon, with wave vector $\vec{k}_p$, to decay into two daughter photons, signal and idler with wave vectors $\vec{k}_{s,i}$, strongly depends on the momentum (wave vector) mismatch $\hbar\vec{\Delta k} \equiv \hbar\vec{k}_s + \hbar\vec{k}_i - \hbar\vec{k}_p$. The allowed mismatch forms an uncertainty relation with the volume over which the nonlinear interaction takes place. Its component parallel to the pump, or longitudinal mismatch $\Delta k_{\parallel}$, is restricted by the inverse length of the nonlinear material. The component perpendicular to the pump, or transverse mismatch $\Delta k_{\perp}$, is restricted by the inverse nonlinear interaction area, generally given by the Gaussian profile of the pump beam.

In a phase-matched process, $\Delta k_{\parallel} = 0$, which is only satisfied in a few nonlinear materials. More generally $\Delta k_{\parallel} \neq 0$, causing pairs to be generated out of phase with respect to pairs generated earlier in the nonlinear material. The relative phase difference depends on the nonlinear interaction length L. If L is equal to an odd multiple of the so-called coherence length $L_c = (\pi/\Delta k_{\parallel})$ [13], the interference between the emitted pairs is fully constructive leading to a local maximum in the emission probability. At $L < L_c$, the pairs are always generated in phase. Moreover, at small L, the allowed longitudinal mismatch is very large, which leads to a very broad spectrum of emitted photons, both in frequency and in angle.

Figure 1(a) shows the allowed mismatch for a thick crystal and an ultrathin layer. While the thick crystal restricts the signal and idler angles and frequencies, the ultrathin layer allows a broad range of modes to be populated. The calculated frequency—angular spectrum for SPDC from a single coherence length or its odd multiple [Figs. 1(c) and 1(d)] is far broader than any phase-matched SPDC spectra observed from a macroscopically thick crystal [Fig. 1(b)]. The emission characteristics differ so greatly between phase-matched and nonphase-matched SPDC that they can be considered separate sources of photon pairs [14].

While the possible emission angles and frequencies for the signal and idler photons are determined by the longitudinal mismatch, the *correlation* between the signal and idler angles of emission is governed by the transverse mismatch [15,16]. These correlations will be tight if the pump has a large beam waist. Similarly, the frequency correlations are governed by the bandwidth of the pump [17,18] and will be tight for a narrow band continuous-wave pump. For this reason, SPDC from an ultrathin layer should produce photon pairs that are highly entangled in angle and frequency: while these parameters are very uncertain for a single photon, they are known with certainty when the conjugate photon is detected. It is noteworthy that
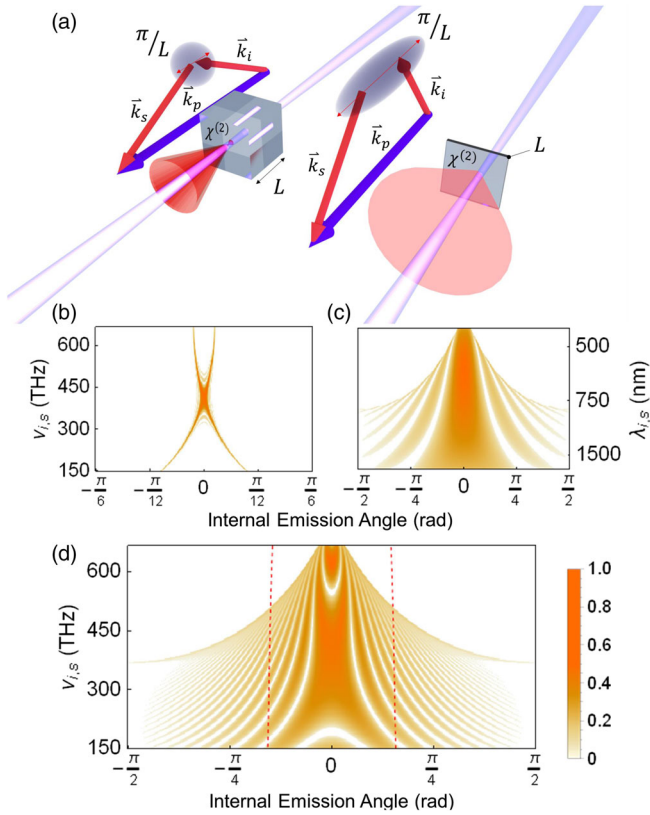
FIG. 1. (a) SPDC in a thick (left) and ultrathin (right) nonlinear layer orthogonal to the pump. Middle panels: the frequency-angular spectrum calculated for a phase-matched type-I BBO crystal with $L = 1$ mm (b) and nonphase-matched type-0 lithium niobate crystal with $L = L_c = 1.37$ μm (c). The pump wavelength is 405 nm and beam waist 100 μm. Note the different x-axis scales between (b) and (c). Panel (d): the frequency-angular spectrum expected for a nonphase-matched type-0 lithium niobate crystal with $L = 5L_c$. Red dashed lines: the angle of internal reflection, which limits the angle collected.

while previous attempts to boost the bipartite entanglement have primarily focused on increasing either frequency or angular entanglement [19,20], SPDC in an ultrathin layer *simultaneously* has gains in both, leading to a massive improvement over previous techniques.

The reduced interaction length, however, leads to a lower SPDC emission probability. This can be partly compensated for by using a highly nonlinear medium. Here, we use an x-cut lithium niobate (LN) crystal and, by taking advantage of the fact that we no longer need to phase match, utilize the large d_{33} component of the nonlinear susceptibility tensor by correctly orienting the pump polarization. The d_{33} component of LN (40 pm/V) is roughly 40 times stronger than the effective susceptibility of β-barium borate (BBO), a standard crystal used for SPDC experiments [13].

The experimental setup is shown in Fig. 2. The sample tested was a thin layer of magnesium oxide doped LN on a 500 μm fused silica substrate. The z axis of LN was in the
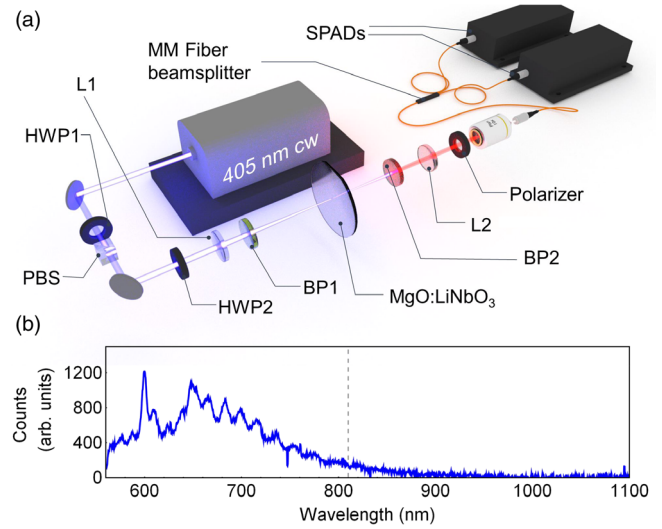
FIG. 2. The setup used to detect SPDC from LN (a) and the fluorescence spectrum measured with a spectrometer (b). The dashed line indicates the degenerate wavelength where most of the measurements were taken.

plane of the layer. The thickness of the sample varied from 5.9 μm to 6.8 μm, due to the nonuniform fabrication of the wafer. Therefore, by scanning the LN in the z-y plane it was possible to tune the length (see Supplemental Material [21]).

Despite the use of the highest nonlinear component available in LN, the efficiency remained much lower than for phase-matched SPDC in a macroscopic crystal. As a result, fluorescence, which can usually be disregarded when working with phase-matched SPDC, became the dominant process in the spectral region of interest. The measured fluorescence [Fig. 2(b)] was more than an order of magnitude stronger than the expected SPDC emission. Because of the broadband nature of nonphase-matched SPDC, distinguishing the two-photon radiation from fluorescence could only be done using correlation measurements.

The correlation measurements were performed using the Hanbury Brown–Twiss setup [Fig. 2(a)]. To begin with, the normalized second-order correlation function $g^{(2)}(\tau)$ was measured and a strong two-photon correlation peak was observed [Fig. 3(a)]. Further, the value of $g^{(2)}(0)$ was measured for different pump powers [Fig. 3(b)]. The measured value of $g^{(2)}(0) - 1$ had an inverse dependence on the pump power, which is a fingerprint of two-photon emission [26]. The correlation function $g^{(2)}(0)$, related to the coincidences-to-accidentals ratio CAR $= g^{(2)}(0) - 1$, had a high value and an inverse dependence on the mean number of photons, both of which are compelling evidence of two-photon light generation.

The measured polarization dependence of the coincidence count rate [Fig. 3(c)] confirms that the SPDC was mediated by the d_{33} component of the nonlinear
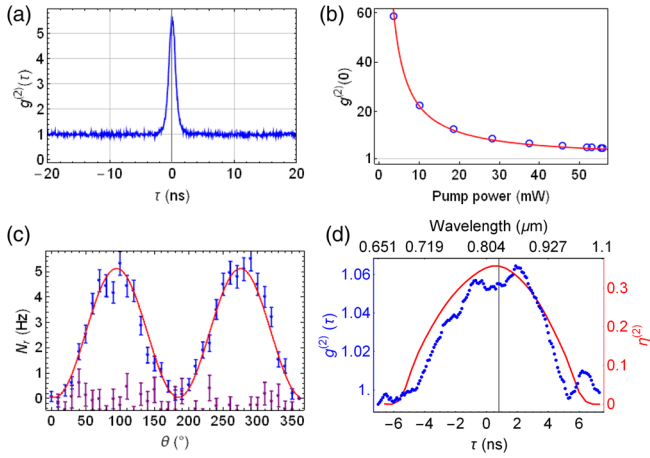
FIG. 3. Two-photon correlations from nonphase-matched SPDC. (a) The normalized two-photon temporal correlation function. (b) The normalized correlation function at zero time delay measured versus the pump power (blue points) and fitted with an inverse dependence (red line). (c) The rate of real coincidences versus the pump polarization direction, for the emission polarized along z (blue points, red fit) and along y (purple points). (d) The normalized temporal correlation function measured after propagation through a dispersive fiber. The temporal delay is mapped into units of wavelength. The double photon quantum efficiency, which limits the collection bandwidth, is shown in red. The gray line indicates the degenerate frequency. (e) The coincidence rate (blue points), for optimized photon pair collection, as a function of the pump power centered at 500 nm with the expected linear power dependence (red).

susceptibility tensor, with the pump, signal, and idler photons all polarized along the z axis. Indeed, the SPDC was noticeable only when the signal and idler photons were polarized along the z axis, in this case the coincidence rate depended on the angle θ between the pump polarization and the y axis as $\sin^2(\theta)$ (blue points, red fit). For the emission polarized along the y axis, no real coincidences (see Supplemental Material [21]) were observed (purple points).

The SPDC spectrum was measured using single-photon spectroscopy [27,28] (see Supplemental Material [21]), which allowed us to distinguish it from the fluorescence spectrum. Light generated from LN was coupled into a dispersive fiber. After propagation through the fiber the two-photon wave packets spread in time. Therefore, the difference in the signal and idler photon detection times could be mapped to a frequency difference. The measured normalized correlation function after the propagation through 160 m of optical fiber is shown in Fig. 3(d). The width of the peak corresponds to 200 nm. This was less than the expected width of 600 nm [Fig. 1(d)] because of the relatively narrow sensitivity range of the single-photon detectors (see Supplemental Material [21]) and frequency-dependent fiber coupling. The biphoton correlation time, given by the inverse spectral width [27], was estimated to be 10 fs. The full spectral range of 600 nm corresponds to a correlation time of 3 fs.

Measurements with a 405 nm pump yielded a modest coincidence count rate due to the high fluorescence background saturating detectors even at low powers. To optimize this we moved to a 500 nm cw pump operating in a similar power range. The shift in wavelength reduced the fluorescence allowing a broader angle of emission to be collected without saturating the detectors. In addition, we tightly focused the pump to reduce the spatial mode content of the SPDC radiation and used a high NA system to collect large emission angles. Both the coincidence rate as a function of pump power and the spectral bandwidth using the single-photon spectroscopy method were measured with the improved system (Fig. 4). With the improved setup the coincidence rate at 220 mW pump power was 1400 Hz, $g^{(2)}(0)$ was 5700 (see Supplemental Material [21]) at 5 mW pump power and the spectral width was measured to be around 150 THz (500 nm).

To demonstrate the high degree of frequency entanglement, we measured the joint spectral intensity (JSI), quantifying the joint probability $P(\omega_s, \omega_i)$ of the signal and idler photons having frequencies ω_s, ω_i, respectively. The JSI was reconstructed using stimulated emission tomography (SET) [29], see Fig. 5(a) and the Supplemental Material [21].

By pumping with the second harmonic of the Nd:YAG laser at 532 nm and tuning the seed beam wavelength between 1500 and 1620 nm, a small part of the JSI [Figs. 5(b) and 5(c)] was mapped out [Fig. 5(d)]. Because of the narrow tuning range of the seed, the full spectral range of SPDC could not be obtained. Still, the SET results demonstrate tight frequency correlations (0.6 ± 0.2 THz, limited by the spectrometer resolution), within a 13 ± 1 THz (limited by the tuning range of the seed) range of the JSI. Using the Fedorov ratio [19,30], given by the ratio of the conditional width and unconditional width of the JSI, the region probed confirms a degree of entanglement of at least 20. This value is a huge underestimation of the true degree of entanglement as
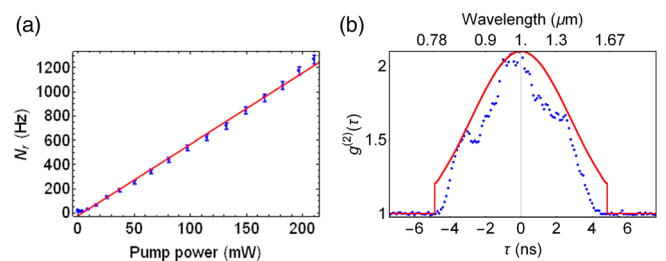
FIG. 4. The two-photon correlations for an optimized collection system pumped at 500 nm. (a) Shows the coincidence rate (blue points) as a function of the pump power, the expected linear dependence is shown in red. (b) The frequency spectrum measured after passing through a 780 nm longpass filter using the single-photon spectroscopy method, the blue points are the values of $g^{(2)}$ as a function of delay time after the biphoton has propagated through a dispersive fiber, the red curve is the calculated frequency spectrum after being cut at 780 nm.
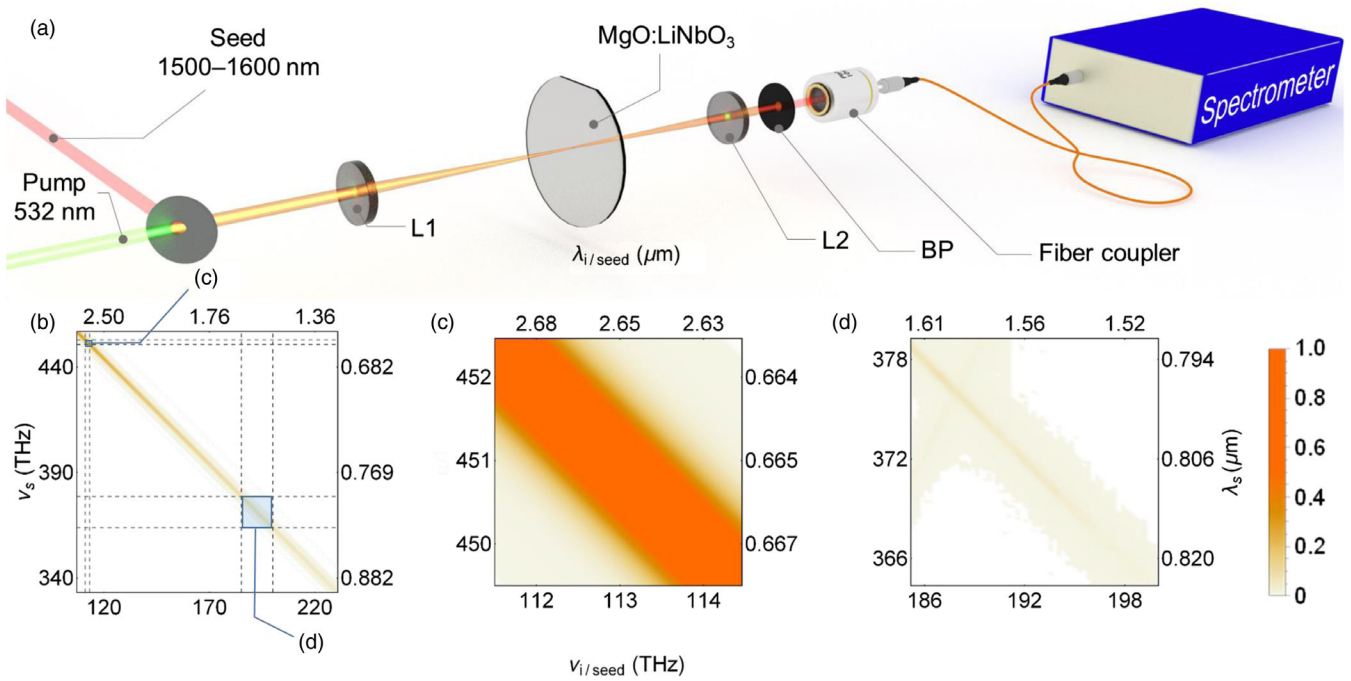
FIG. 5. The setup for the SET measurement (a) and the calculated JSI for 5.8 μm LN pumped at 532 nm (b), with an enlarged interval (c) to emphasize the small width. $L1$ and $L2$ are lenses and BP is a bandpass filter blocking the pump and the seed. Panel (d) shows a fragment of JSI measured using SET, with the bounds limited by the tunability of the seed. The fainter line with a positive tilt in (d) is due to second harmonic generation of the seed.

we cannot account for the broad spectral width and phase information. From the simulated JSI [Fig. 5(b)] we anticipate, by using the Fedorov ratio again, the degree of entanglement will be around 2 orders of magnitude larger than stated.

Generating entangled photons with a broad spectral and angular width has been a long-standing goal in quantum optics [31–33]. Highly nonlinear ultrathin layers provide both a platform on which to achieve this goal and, due to their size and scale, a platform on which to design miniaturized quantum-photonic chips [34]. To our knowledge, here we have reported the smallest source of SPDC (6 μm $\times$ 10 μm $\times$ 10 μm) found to date. Several semiconductor materials, such as gallium arsenide, have much higher second-order susceptibilities than that of LN [35]. In addition, structuring such materials to enhance their resonance response can further improve the SPDC efficiency [36], thus allowing even thinner samples to be made.

The two-photon time and space correlation widths, proportional to the inverse spectral and angular widths, respectively, promise to be tighter than anything currently observed. As such, the correlations in space and time could become a new resolution standard. While the ultrashort correlation time can be used to synchronize distant clocks [7], the tight spatial correlations can dramatically improve the resolution of many quantum imaging techniques such as ghost imaging and imaging with undetected photons [1–3,37]. In two-photon microscopy, such a source will

allow imaging well beyond the diffraction limit [38], as the resolution will be determined only by the interaction length.

Both the angle of emission and frequency can be used as variables for encoding quantum information [39,40]. Because of the huge spectral and angular widths of non-phase-matched SPDC, the expected degree of entanglement, and thus the information capacity, for nonphase-matched SPDC is almost an order of magnitude higher than for a phase-matched process. Additionally, using the principle of hyperentanglement, whereby the biphoton state is entangled in more than one degree of freedom [41], the nonphase-matched state increases the information capacity as the product of both the entanglement in the frequency and angular domain, leading to improvements by several orders of magnitude.

Finally, we expect that highly nonlinear thin layers will also be suitable platforms on which to observe higher-order parametric down-conversion effects, such as the generation of three-photon states from a cubic interaction [42]. Phase matching for higher-order processes becomes increasingly challenging due to the larger refractive index difference between the pump photon and daughter photons. This restricts the number of nonlinear materials to work with to a far greater extent than for second-order processes. Therefore, working in the nonphase-matched regime is a reasonable trade-off as it allows one to utilize materials with a huge cubic susceptibility.

*cameron.okoth@mpl.mpg.de

[1] G. B. Lemos, V. Borish, G. D. Cole, S. Ramelow, R. Lapkiewicz, and A. Zeilinger, Quantum imaging with undetected photons, Nature (London) **512**, 409 (2014).

[2] T. B. Pittman, Y. H. Shih, D. V. Strekalov, and A. V. Sergienko, Optical imaging by means of two-photon quantum entanglement, Phys. Rev. A **52**, R3429 (1995).

[3] G. Brida, M. Genovese, and I. R. Berchera, Experimental realization of sub-shot-noise quantum imaging, Nat. Photonics **4**, 227 (2010).

[4] Y. Adachi, T. Yamamoto, M. Koashi, and N. Imoto, Simple and Efficient Quantum Key Distribution with Parametric Down-Conversion, Phys. Rev. Lett. **99**, 180503 (2007).

[5] T. Jennewein, C. Simon, G. Weihs, H. Weinfurter, and A. Zeilinger, Quantum Cryptography with Entangled Photons, Phys. Rev. Lett. **84**, 4729 (2000).

[6] L.-A. Wu, H. J. Kimble, J. L. Hall, and H. Wu, Generation of Squeezed States by Parametric Down Conversion, Phys. Rev. Lett. **57**, 2520 (1986).

[7] A. Valencia, G. Scarcelli, and Y. Shih, Distant clock synchronization using entangled photon pairs, Appl. Phys. Lett. **85**, 2655 (2004).

[8] Y. H. Shih and C. O. Alley, New Type of Einstein-Podolsky-Rosen-Bohm Experiment Using Pairs of Light Quanta Produced by Optical Parametric Down Conversion, Phys. Rev. Lett. **61**, 2921 (1988).

[9] H. D. Saleh, S. Vezzoli, L. Caspani, A. Branny, S. Kumar, B. D. Gerardot, and D. Faccio, Towards spontaneous parametric down conversion from monolayer MoS$_2$, Sci. Rep. **8**, 3862 (2018).

[10] M. Tokman, Z. Long, S. AlMutairi, Y. Wang, V. Vdovin, M. Belkin, and A. Belyanin, Purcell enhancement of the parametric down-conversion in two-dimensional nonlinear materials, APL Photonics **4**, 034403 (2019).

[11] S. Yamashita, Nonlinear optics in carbon nanotube, graphene, and related 2D materials, APL Photonics **4**, 034301 (2019).

[12] G. Marino, A. S. Solntsev, L. Xu, V. F. Gili, L. Carletti, A. N. Poddubny, M. Rahmani, D. A. Smirnova, H. Chen, G. Zhang *et al.*, Spontaneous photon-pair generation at the nanoscale, Optica **6**, 1416 (2019).

[13] R. W. Boyd, *Nonlinear Optics* (Elsevier, Milton Keynes, 2003).

[14] C. Yuan, W. Zhang, and Y. Huang, Spatiotemporally separable biphoton state generated by spontaneous four wave mixing in ultrathin nonlinear films, arXiv:1903.10936.

[15] A. V. Burlakov, M. V. Chekhova, D. N. Klyshko, S. P. Kulik, A. N. Penin, Y. H. Shih, and D. V. Strekalov, Interference effects in spontaneous two-photon parametric scattering from two macroscopic regions, Phys. Rev. A **56**, 3214 (1997).

[16] C. H. Monken, P. H. Souto Ribeiro, and S. Pádua, Transfer of angular spectrum and image formation in spontaneous parametric down-conversion, Phys. Rev. A **57**, 3123 (1998).

[17] T. E. Keller and M. H. Rubin, Theory of two-photon entanglement for spontaneous parametric down-conversion driven by a narrow pump pulse, Phys. Rev. A **56**, 1534 (1997).

[18] W. P. Grice and I. A. Walmsley, Spectral information and distinguishability in type-ii down-conversion with a broad-band pump, Phys. Rev. A **56**, 1627 (1997).

[19] M. V. Fedorov, M. A. Efremov, P. A. Volkov, E. V. Moreva, S. S. Straupe, and S. P. Kulik, Anisotropically and High Entanglement of Biphoton States Generated in Spontaneous Parametric Down-Conversion, Phys. Rev. Lett. **99**, 063901 (2007).

[20] G. Brida, V. Caricato, M. V. Fedorov, M. Genovese, M. Gramegna, and S. P. Kulik, Characterization of spectral entanglement of spontaneous parametric-down conversion biphotons in femtosecond pulsed regime, Europhys. Lett. **87**, 64003 (2009).

[21] See Supplemental Material at http://link.aps.org/supplemental/10.1103/PhysRevLett.123.263602 for experimental methods and sample details, which includes Refs. [22–25].

[22] Y. M. Mikhailova, P. A. Volkov, and M. V. Fedorov, Biphoton wave packets in parametric down-conversion: Spectral and temporal structure and degree of entanglement, Phys. Rev. A **78**, 062327 (2008).

[23] M. Hendrych, M. Micuda, and J. Torres, Tunable control of the frequency correlations of entangled photons, Opt. Lett. **32**, 2339 (2007).

[24] R. Newman, Visible light from a silicon *p-n* junction, Phys. Rev. **100**, 700 (1955).

[25] ECD-X documentation, http://www.m2lasers.com/images/Datasheet_SolsTiS_ECD-X.pdf.

[26] O. A. Ivanova, T. S. Iskhakov, A. N. Penin, and M. V. Chekhova, Multiphoton correlations in parametric down-conversion and their measurement in the pulsed regime, Quantum Electron. **36**, 951 (2006).

[27] A. Valencia, M. V. Chekhova, A. Trifonov, and Y. Shih, Entangled Two-Photon Wave Packet in a Dispersive Medium, Phys. Rev. Lett. **88**, 183601 (2002).

[28] M. Avenhaus, A. Eckstein, P. J. Mosley, and C. Silberhorn, Fiber-assisted single-photon spectrograph, Opt. Lett. **34**, 2873 (2009).

[29] M. Liscidini and J. E. Sipe, Stimulated Emission Tomography, Phys. Rev. Lett. **111**, 193602 (2013).

[30] M. V. Fedorov, M. A. Efremov, A. E. Kazakov, K. W. Chan, C. K. Law, and J. H. Eberly, Packet narrowing and quantum entanglement in photoionization and photodissociation, Phys. Rev. A **69**, 052117 (2004).

[31] M. B. Nasr, S. Carrasco, B. E. A. Saleh, A. V. Sergienko, M. C. Teich, J. P. Torres, L. Torner, D. S. Hum, and M. M. Fejer, Ultrabroadband Biphotons Generated via Chirped Quasi-Phase-Matched Optical Parametric Down-Conversion, Phys. Rev. Lett. **100**, 183601 (2008).

[32] C. Bernhard, B. Bessire, T. Feurer, and A. Stefanov, Shaping frequency-entangled qudits, Phys. Rev. A **88**, 032322 (2013).

[33] K. G. Katamadze, N. A. Borshchevskaya, I. V. Dyakonov, A. V. Paterova, and S. P. Kulik, Broadband biphotons in a single spatial mode, Phys. Rev. A **92,** 023812 (2015).

[34] X. Guo, C.-l. Zou, C. Schuck, H. Jung, R. Cheng, and H. X. Tang, Parametric down-conversion photon-pair source on a nanophotonic chip, Light: Sci. Appl. **6,** e16249 (2017).

[35] V. G. Dmitriev, G. G. Gurzadyan, and D. N. Nikogosyan, *Handbook of Nonlinear Optical Crystals* (Springer, Berlin, 1999), Vol. 64.

[36] S. Liu, P. P. Vabishchevich, A. Vaskin, J. L. Reno, G. A. Keeler, M. B. Sinclair, I. Staude, and I. Brener, An all-dielectric metasurface as a broadband optical frequency mixer, Nat. Commun. **9,** 2507 (2018).

[37] M. DAngelo, A. Valencia, M. H. Rubin, and Y. Shih, Resolution of quantum and classical ghost imaging, Phys. Rev. A **72,** 013810 (2005).

[38] W. Denk, J. H. Strickler, and W. W. Webb, Two-photon laser scanning fluorescence microscopy, Science **248,** 73 (1990).

[39] L. Olislager, J. Cussey, A. T. Nguyen, P. Emplit, S. Massar, J.-M. Merolla, and K. P. Huy, Frequency-bin entangled photons, Phys. Rev. A **82,** 013804 (2010).

[40] J. G. Rarity and P. R. Tapster, Experimental Violation of Bells Inequality Based on Phase and Momentum, Phys. Rev. Lett. **64,** 2495 (1990).

[41] J. T. Barreiro, N. K. Langford, N. A. Peters, and P. G. Kwiat, Generation of Hyperentangled Photon Pairs, Phys. Rev. Lett. **95,** 260501 (2005).

[42] C. Okoth, A. Cavanna, N. Y. Joly, and M. V. Chekhova, Seeded and unseeded high-order parametric down-conversion, Phys. Rev. A **99,** 043809 (2019).